Zero energy and chiral edge modes in a *p*-wave magnetic spin model

G. Kells[1] and J. Vala[1,2]
[1]*Department of Mathematical Physics, National University of Ireland, Maynooth, Ireland*
[2]*School of Theoretical Physics, Dublin Institute for Advanced Studies, 10 Burlington Road, Dublin, Ireland*
(Received 29 June 2010; revised manuscript received 5 August 2010; published 22 September 2010)

In this work we discuss the formation of zero energy vortex and chiral edge modes in a fermionic representation of the Kitaev honeycomb model. We introduce the representation and show how the associated Jordan-Wigner procedure naturally defines the so-called branch cuts that connect the topological vortex excitations. Using this notion of the branch cuts we show how to, in the non-Abelian phase of the model, describe the Majorana zero mode structure associated with vortex excitations. Furthermore we show how, by intersecting the edges between Abelian and non-Abelian domains, the branch cuts dictate the character of the chiral edge modes. In particular we will see in what situations the exact zero energy Majorana edge modes exist. On a cylinder, and for the particular instances where the Abelian phase of the model is the full vacuum, we have been able to exactly solve for the systems edge energy eigensolutions and derive a recursive formula that exactly describes the edge mode structure. Penetration depth is also calculated and shown to be dependent on the momentum of the edge mode. These solutions also describe the overall character of the fully open non-Abelian domain and are excellent approximations at moderate distances from the corners.

DOI: 10.1103/PhysRevB.82.125122 PACS number(s): 05.30.Pr, 75.10.Jm, 03.65.Vf

I. INTRODUCTION

Two-dimensional (2D) fermion models that display spinless *p*-wave pairing are the subject of recent intense interest. This curiosity is due largely to the potential technological applications associated with (A) its Abelian phase, (B) its non-Abelian phase, and (C) domain walls between Abelian and non-Abelian regimes. The Abelian phase has the potential for use in fault tolerant quantum information storage.[1] However, the majority of the interest is because these *p*-wave systems can potentially support the Majorana zero modes that give rise to non-Abelian statistics,[2–6] and the fact that the domain wall between these phases also supports Majorana and chiral edge modes.[2,6] These later properties could potentially be used in quantum information processing devices that are naturally protected from noise, see, for example, Refs. 7 and 8.

The understanding of these properties has been enhanced through the use of exactly or nearly solvable spin models. Arguably the most important for the spinless *p*-wave system is the Kitaev honeycomb system.[9] The Abelian phase of model can be analyzed using perturbation theory[9–11] and is reduced to the so-called "toric code" system in this limit.[1] The main advantage of this system however is that it can be understood as either Majorana[9,12–14] or Dirac fermions[15–20] hopping in a $\mathbb{Z}_2$ gauge field. In the Dirac fermion picture, obtained using Jordan-Wigner-type fermionization procedures, the spin Hamiltonian in each gauge sector reduces exactly to a mean-field-type *p*-wave system[18] but where the fermionic vacuum is exactly that of the toric code.[20] The overall aim of this paper is to present an alternative explanation for the zero and low-energy chiral modes that exist in this system. Our perspective is complementary to previous work on the honeycomb model edge states (see, for example, Ref. 9 Appendix B and Ref. 16), the continuum *p*-wave analysis of Refs. 2 and 6, and the bosonic condensation theory presented in Refs. 21 and 22.

The first half of the paper describes how the notion of a branch cut can arise naturally from the 2D Jordan-Wigner procedure. This is in contrast with mean-field *p*-wave analysis where the branch cuts are an afterthought to ensure that the modes are single valued. We will see that, as expected, these branch cuts connect the topological defects (vortices) of the system. However, through out this story we will attempt to emphasize that it is the branch cuts that are the fundamental objects. For example, it is the branch cuts, and not the vortices, that dictate the fermionic behavior of the system. This perspective also holds on the boundaries between Abelian and non-Abelian domains. For example, we will see that it is the number of branch cuts through those edges that dictate the character of the modes found there. In the second half of the paper we will analyze the zero energy bulk modes and the zero energy and chiral edge modes found in the model. Our analysis of edge modes is valid for both cylindrical and fully open boundary conditions but is based on the consistency relations between homologically trivial excitations (vortices) and the homologically nontrivial excitations on a torus.[20] We first introduce the cylindrical system and describe the general character of the modes found in this case. The general conclusion is that exact zero modes only form on edges that are intersected by an even number of branch cuts. In addition to this we see for the hard boundary condition (i.e., where the Abelian domain is exactly the vacuum), that there are exact solutions for the Bogoliubov-de Gennes (BdG) equations. We use these solutions to examine the mode penetration depth as a function of the Hamiltonian parameters and the mode momenta along the edge.

We finally extend the general analysis to fully open rectangular boundary conditions we see that exact zero modes only form in this case when there is an *odd* number of branch cuts through the domain. The reason for the difference is an extra phase factor that is contributed at the corners of the system. At moderate distances from the corners however the exact solutions for the cylindrical hard boundary system are an excellent approximation for the open system eigenmodes.

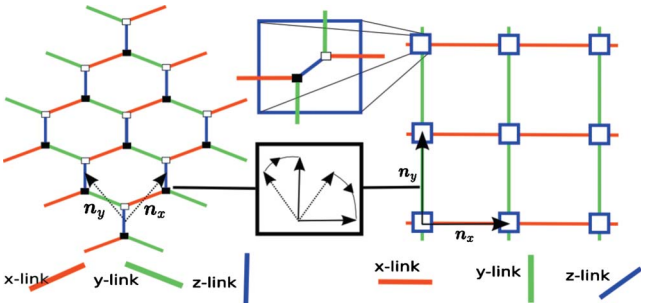

FIG. 1. (Color online) The hexagonal spin representation and the square hard-core boson/effective spin representation.

These results are in general agreement with Refs. 2 and 9.

Spin Hamiltonian and loop symmetries

The Kitaev honeycomb system consists of spins on the sites of a hexagonal lattice. The Hamiltonian can be written as

$$H_0 = -\sum_{\alpha\in\{x,y,z\}}\sum_{i,j} J_\alpha K^\alpha_{i,j}, \tag{1}$$

where $K^\alpha_{ij}=\sigma^\alpha_i\sigma^\alpha_j$ denotes a directional spin exchange interaction occurring between the sites i,j connected by a α link, see Fig. 1. We define a unit cell of the lattice with the two unit vectors $\boldsymbol{n}_x$ and $\boldsymbol{n}_y$ as shown in Fig. 1. By contracting each z link to a single point we define the position vector labeling the z dimers on a square lattice as $\boldsymbol{q}=q_x\boldsymbol{n}_x+q_y\boldsymbol{n}_y$.

Consider now products of K operators along loops on the lattice, $K^{\alpha^{(1)}}_{ij}K^{\alpha^{(2)}}_{jk}\cdots K^{\alpha^{(n)}}_{li}$, where $\alpha^{(m)}\in x,y,z$. Any loop constructed in this way commutes with the Hamiltonian and with all other loops. The shortest such loop symmetries are the plaquette operators,

$$\boldsymbol{W}_{\boldsymbol{q}} = \sigma^z_1\sigma^x_2\sigma^y_3\sigma^z_4\sigma^x_5\sigma^y_6, \tag{2}$$

where the numbers 1 through 6 label lattice sites on single hexagonal plaquette. We will use the convention that $\boldsymbol{q}$ denotes the z dimer directly below the plaquette. The fact that the Hamiltonian commutes with all plaquette operators implies that we may choose energy eigenvectors $|n\rangle$ such that $W_{\boldsymbol{q}}=\langle n|\boldsymbol{W}_{\boldsymbol{q}}|n\rangle=\pm 1$. If $W_{\boldsymbol{q}}=-1$ then we say that the state $|n\rangle$ carries a vortex at $\boldsymbol{q}$. When we refer to a particular vortex sector we mean the subspace of the system with a particular configuration of vortices. The vortex-free sector, for example, is the subspace spanned by all eigenvectors such that $W_{\boldsymbol{q}}=1$ for all $\boldsymbol{q}$.

The breaking of T symmetry is essential for relating the model to chiral p-wave superconductors. Following the work of Refs. 9, 12, and 13 we use the three-body term,

$$H_1 = -\kappa\sum_{\boldsymbol{q}}\sum_{l=1}^{6} P^{(l)}_{\boldsymbol{q}} \tag{3}$$

with the second summation running over the six terms,

$$\sum_{l=1}^{6} P^{(l)}_{\boldsymbol{q}} = \sigma^x_1\sigma^y_6\sigma^z_5 + \sigma^z_2\sigma^y_3\sigma^x_4 + \sigma^y_1\sigma^x_2\sigma^z_3 + \sigma^y_4\sigma^x_5\sigma^z_6 + \sigma^x_3\sigma^z_4\sigma^y_5 + \sigma^y_2\sigma^z_1\sigma^x_6. \tag{4}$$

For simplicity, in this work we will retain only terms $P^{(1)}$, $P^{(2)}$, $P^{(3)}$, and $P^{(4)}$. These terms are sufficient to generate the required non-Abelian phase and in some instances allow for an exact analytical description of the free fermionic modes.

II. FERMIONIC FORMULATION

It was shown in Ref. 20 that each vortex sector of the honeycomb lattice model can be written as a system of fermions hopping on a square lattice in a $\mathbb{Z}_2$ gauge field. The representation has one key advantage over other fermionization methods, namely, the resolution of the system vacua as toric code[1] states. This opens a possible bridge between the non-Abelian anyons of the fermionic p-wave system and recent mathematical constructions using toric code superpositions[23] and lattice dislocations and twists.[24]

Using this fermionization technique,[20] reviewed briefly in the Appendix, we arrive at the following expression for Hamiltonian (1):

$$H_0 = J_x\sum_{\boldsymbol{q}} \boldsymbol{X}_{\boldsymbol{q}}(c^\dagger_{\boldsymbol{q}}-c_{\boldsymbol{q}})(c^\dagger_{\boldsymbol{q}\rightarrow}+c_{\boldsymbol{q}\rightarrow}) + J_y\sum_{\boldsymbol{q}} \boldsymbol{Y}_{\boldsymbol{q}}(c^\dagger_{\boldsymbol{q}}-c_{\boldsymbol{q}})(c^\dagger_{\boldsymbol{q}\uparrow}+c_{\boldsymbol{q}\uparrow}) + J_z\sum_{\boldsymbol{q}}(2c^\dagger_{\boldsymbol{q}}c_{\boldsymbol{q}}-I), \tag{5}$$

where here and in future we use the shorthand $\boldsymbol{q}\rightarrow=\boldsymbol{q}+n_x$, $\boldsymbol{q}\uparrow=\boldsymbol{q}+n_y$, and $\boldsymbol{q}\nearrow=\boldsymbol{q}+n_y+n_x$. In the plane, $\boldsymbol{Y}_{\boldsymbol{q}}=I$ for all $\boldsymbol{q}$ and $\boldsymbol{X}_{\boldsymbol{q}}$ is defined as

$$\boldsymbol{X}_{x,y} \equiv \prod_{y'=0}^{y-1} \boldsymbol{W}_{x,y'}. \tag{6}$$

The terms $P^{(l)}$ in Eq. (4) are the T-symmetry breaking terms, the fermionic form of which was also derived in Ref. 20. As we mentioned above in this work we will retain only the first four terms,

$$P^{(1)}_{\boldsymbol{q}} = -i\kappa\boldsymbol{X}_{\boldsymbol{q}}(c^\dagger_{\boldsymbol{q}}-c_{\boldsymbol{q}})(c^\dagger_{\boldsymbol{q}\rightarrow}-c_{\boldsymbol{q}\rightarrow}),$$

$$P^{(2)}_{\boldsymbol{q}} = -i\kappa\boldsymbol{X}_{\boldsymbol{q}\uparrow}(c^\dagger_{\boldsymbol{q}\uparrow}+c_{\boldsymbol{q}\uparrow})(c^\dagger_{\boldsymbol{q}\nearrow}+c_{\boldsymbol{q}\nearrow}),$$

$$P^{(3)}_{\boldsymbol{q}} = +i\kappa\boldsymbol{Y}_{\boldsymbol{q}}(c^\dagger_{\boldsymbol{q}}-c_{\boldsymbol{q}})(c^\dagger_{\boldsymbol{q}\uparrow}-c_{\boldsymbol{q}\uparrow}),$$

$$P^{(4)}_{\boldsymbol{q}} = +i\kappa\boldsymbol{Y}_{\boldsymbol{q}\rightarrow}(c^\dagger_{\boldsymbol{q}\rightarrow}+c_{\boldsymbol{q}\rightarrow})(c^\dagger_{\boldsymbol{q}\nearrow}+c_{\boldsymbol{q}\nearrow}). \tag{7}$$

The Jordan-Wigner convention used to define the fermions is directly responsible for how vorticity is encoded in the fermionic system. For the string convention chosen in Ref. 20 the vorticity is encoded in the fermionic Hamiltonian through condition (6). On a torus there are additional homologically nontrivial degrees of freedom which also need to be determined consistently with condition (6). These homologically nontrivial degrees of freedom are encoded in the $X_{\boldsymbol{q}}$ and $Y_{\boldsymbol{q}}$ values at the boundary of the system.[20] Recently we have

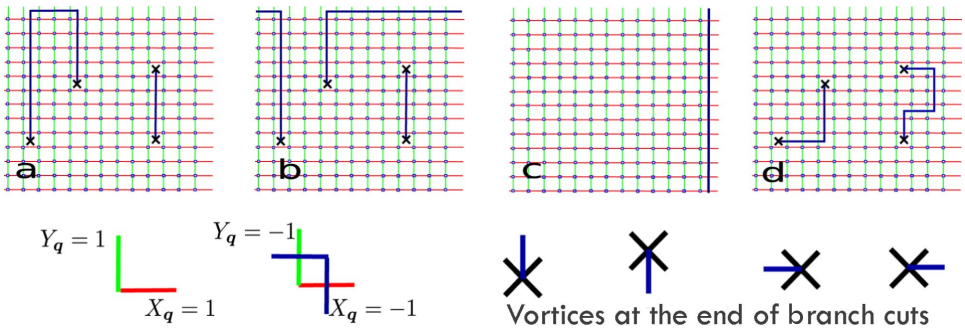

FIG. 2. (Color online) Vortices always appear at the end of a branch cut. (a)–(c) are real vortex configurations. Note that on a torus the topological sectors can also be encoded as branch cuts and their values dictate which vortices are connected to each other. With the conventions used in Ref. 20 the term $Y_{(N_y,0)}=-1$ dictates which vortices are connected by the branch cuts. In the absence of any vortices the x and y antiperiodic homological conditions are encoded as lines $X_{(N_x,y)}=-1 \ \forall y$ and $Y_{(N_y,x)}=-1 \ \forall x$, respectively. For example, in (c) the branch cut on the right-hand side indicates that the sector is antiperiodic along the n_x direction. (d) is a "simulated" vortex configurations obtained by locally varying couplings J_x and J_y and κ.

extended this Jordan-Wigner method to deal with the Yao-Kivelson 3-12 lattice variant of the model.[25]

The consistency relations provided in Ref. 20 have an interesting pictorial representation which leads us naturally to the concept of branch cuts and a less restrictive understanding of vorticity. For any vortex arrangement we see that there are lines of $X_q=-1$ and $Y_q=-1$ which together connect vortices in pairs. A number of examples are given in Fig. 2.

On an open plane we no longer have these homologically nontrivial symmetries but neither do we have the condition that vortices are created in pairs: $\Pi_q W_q=1$. In this case valid vortex sectors can be encoded using the following guidelines. (1) The vortex free sector ($W_q=1 \forall q$) is encoded as $X_q=1 \ \forall q$. (2) A single isolated vortex at position q is encoded with $X_q=1$ everywhere except for a single line of $X_{x,y}=-1$ starting at $y+n_y$ and extending to infinity. (3) When two vortices occur at different x positions there are two unique strands of $X_q=-1$ connecting them both to infinity. (4) If two vortices occur at different y-positions and with the same x-position then a vertical line of $X_q=-1$ connects them.

One can "simulate" the change in vortex sectors by altering the coupling constants (the J_x and J_y) on unique links.[26] Thus by changing the sign of J_x at q one effectively changes the gauge encoding X_q. Strictly speaking this does not change the vortex sector of the Hamiltonian however. With our fermionization convention, and on a plane, there are no vortex sectors that correspond to setting $J_y \to -J_y$ at q.

With this perspective it is easier to appreciate that truly meaningful objects in this story are not the vortices themselves but the connected strings of -1's defined on the X_q and Y_q matrices. Indeed as we have already shown these strings take on the role of branch cuts in our fermionic Hamiltonian and will see later that it is their ends that give rise to localized zero modes. From this perspective we can say that zero modes are only associated with vortices because a branch cut always happens to end there. Furthermore we will see that the precise structure of unpaired Majorana modes that live on the domains between Abelian and non-Abelian phases depends on the number of branch cuts intersecting the edge and not in general on the number or position of the vortices inside the non-Abelian bulk.

From now on we will take $J=J_x=J_y$, dropping the subscript and take the viewpoint used in Ref. 26 where, by changing the coupling strengths, we can simulate changing the vortex configurations. In what follows however, and only for convenience, we will generally continue to regard the J and κ terms as constant across the lattice and allow vorticity to be encoded in the X and Y terms. The parameter J dictates which phase we are in. For $J<J_z/2$ we are in the Abelian phase and for $J>J_z/2$ we are in the non-Abelian phase if $\kappa \neq 0$. In what follows we will specify the J and κ values in the Abelian domains as J_A and κ_A, respectively.

III. BULK MAJORANA FERMION ZERO MODES

In this section we will briefly discuss the bulk Majorana modes found at the end of the branch cuts. We will not however discuss the detailed structure of the bulk modes other than to present some numerical calculations. In later sections however we will demonstrate how the structure can be seen as a limiting case of edge modes found between domains of Abelian and non-Abelian topological phase.

We begin by presenting the BdG formalism. The full position space Hamiltonian can be written in the form

$$H = \frac{1}{2}\sum_{qq'} \begin{bmatrix} c_q^\dagger & c_q \end{bmatrix} \begin{bmatrix} \xi_{qq'} & \Delta_{qq'} \\ \Delta_{qq'}^\dagger & -\xi_{qq'}^T \end{bmatrix} \begin{bmatrix} c_{q'} \\ c_{q'}^\dagger \end{bmatrix}. \tag{8}$$

This system can be diagonalized by solving the Bogoliubov-de Gennes eigenvalue problem,

$$\begin{bmatrix} \xi & \Delta \\ \Delta^\dagger & -\xi^T \end{bmatrix} = \begin{bmatrix} U & V^* \\ V & U^* \end{bmatrix} \begin{bmatrix} E & \mathbf{0} \\ \mathbf{0} & -E \end{bmatrix} \begin{bmatrix} U & V^* \\ V & U^* \end{bmatrix}^\dagger, \tag{9}$$

where the nonzero entries of the diagonal matrix $E_{nm}=E_n\delta_{nm}$ are the quasiparticle excitation energies. The Bogoliubov-Valatin quasiparticle excitations are

$$[a_1^\dagger, \ldots, a_M^\dagger, \ a_1, \ldots, a_M] = [c_1^\dagger, \ldots, c_M^\dagger, \ c_1, \ldots, c_M] \times \begin{bmatrix} U & V^* \\ V & U^* \end{bmatrix}, \tag{10}$$

which after inversion and substitution into Eq. (8) give

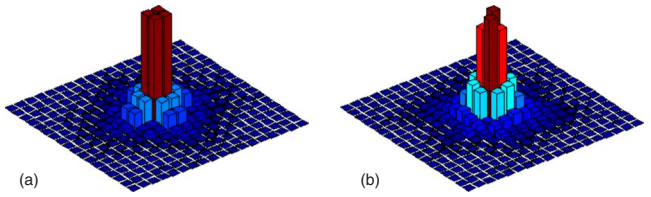

FIG. 3. (Color online) The position space structure $|u_q|=|v_q|$ of vortex Majorana zero modes for (a) $J_z=1$, $J=1$, and $\kappa=0.5$ and (b) $J_z=1$ $J=0.8$, and $\kappa=0.2$.

$$H=\sum_{n=1}^{M} E_n\left(a_n^\dagger a_n-\frac{1}{2}\right). \tag{11}$$

In the non-Abelian phase it is guaranteed by an index theorem[27] that for $2N$ well-separated vortices we have $2N$ zero energy ($E=0$) eigenvalues. N of these eigenvalues are identified with $a^\dagger$'s and N are identified with a's. It is rather remarkable that one can always choose a superposition of the $2N$ $a^\dagger$ and a zero modes such that the resulting modes are fully localized around the vortex excitations,

$$\gamma_j=\sum_{n=1}^{N}\alpha_{jn}a_n^\dagger+\alpha_{j,n+N}a_n=[c_1^\dagger,\ldots,c_M^\dagger,\quad c_1,\ldots,c_M]\begin{bmatrix}u_{q,j}\\ v_{q,j}\end{bmatrix}. \tag{12}$$

A full Dirac fermion can be made from a superposition of two of these localized modes. The localized modes are thus, in a sense, "half" of a Dirac fermion and the supporting vortices are sometimes called "half quantum vortices." As the Dirac fermion mode is split between well-separated locations it cannot interact with local error processes. It is this feature that make these types of systems potentially useful for quantum information processing.

It is interesting that the localization condition also enforces the condition that $u_{qj}=e^{i\Omega_n}v_{qj}^*$. However, if one wishes to call this a Majorana mode $\gamma_j=\gamma_j^\dagger$ it is necessary to multiply the states $(u,v)^T$ by the overall phase $e^{-i\Omega_n/2}$ such that $u_{q,j}=v_{q,j}^*$. It was pointed out by Stone and Chung[5] that the Majorana condition therefore fixes the global phase of the states γ_j up to an overall sign ± 1. Understanding how and when this overall sign changes is crucial to understanding how non-Abelian statistics arise in this degenerate subspace. In Fig. 3 we show the $|u_q|$ and $|v_q|$ position space structure for some different values of J and κ.

IV. MAJORANA AND CHIRAL EDGE STATES

The non-Abelian phase of the honeycomb system is a topological insulator of the BdG class.[28] Roughly speaking this means that we have a bulk energy spectrum which is "insulating" (does not cross the Fermi energy at $E=0$) and an edge spectrum which is "conducting" (does cross the Fermi energy at $E=0$), see, for example, Refs. 9 and 16. For a careful choice of edge conditions it is possible to analytically treat the conducting edge modes.

In order to determine the structure of the modes let us consider an element of an arbitrary eigenstate $a_n^\dagger$ of the BdG Hamiltonian. Each value $u_{x,y}$ is connected to $u_{x\pm1,y}$ and $u_{x,y\pm1}$ through the nonzero elements of the ξ matrix and to $v_{x\pm1,y}$ and $v_{x,y\pm1}$ through the nonzero elements of the Δ matrix. It is quite difficult to say anything generic about the form that an eigenvector should have. One feature is universal however. We see that if the elements around the point $u_{x,y}$ are almost zero then $u_{x,y}$ should also be almost zero. It is true regardless of the values we give our coefficients in our Hamiltonian and it is this rule that determines the vast majority of the zero-mode structure (or lack of it).

In the absence of branch cuts, there is a simple condition that the nine interconnected elements must obey if they are to be eigenstates of the system,

$$\begin{aligned}(2J_z-E)u_{x,y}+J(u_{x+1,y}+u_{x-1,y}+u_{x,y+1}+u_{x,y-1})\\ +(J-2i\kappa)v_{x+1,y}+(-J+2i\kappa)v_{x-1,y}+(J+2i\kappa)v_{x,y+1}\\ +(-J-2i\kappa)v_{x,y-1}=0.\end{aligned} \tag{13}$$

For edge states on a cylinder we make the reasonable assumption that, in the direction of edge, our modes are plane waves (momentum eigenstates). For example, along the lower edge of a cylindrical non-Abelian domain we have BdG excitations of the form

$$a_n^\dagger=\mathcal{N}\sum_q e^{\pm ik_x x}[u(y-y_0)c_q^\dagger+v(y-y_0)c_q], \tag{14}$$

where $\mathcal{N}$ is some normalizing factor. This state corresponds to a superposition of left (right) moving particles and right (left) moving holes.[31] On a cylinder the allowed values of k_x are $2n\pi/N_x$ when there is an even number of branch cuts through the edge and $2(n+1/2)\pi/N_x$ when the number is odd. The basic reasoning is this. A branch cut is accommodated in Eq. (13) by a change in signs of the elements J and κ acting on some (not all) of the values u_q and v_q. To keep the energy low then the phase of the mode $a_n^\dagger$ should abruptly change sign at these locations to counteract the sudden sign change in the fermionic Hamiltonian.

On a cylinder this has interesting consequences. Let us start from the toroidal case and open up the y boundary above and below the $y=0$ line. We now have two edges which are some distance apart. Translation invariance remains in the x direction but is broken in the y direction. Recall now that the antiperiodic x-boundary condition is encoded as a single line of $X_q=-1$. Thus in the periodic vortex free sector we therefore have chiral edge states with $k_x=\pm 2n\pi/N_x$. This includes *two* edge zero modes, one on each edge. In the antiperiodic vortex free case we have no zero modes. This is because we have a single branch cut intersecting both edges and thus $k_x=\pm 2(n+1/2)\pi/N_x$.

If a single vortex exists inside the cylinder there must be a branch cut connecting it to either infinity or some other vortex outside the cylinder. If we were originally in the periodic system then the introduction of a branch cut through one wall would destroy periodicity on this edge and we could not have Majorana zero modes. The other edge however would remain unaffected. In the opposite sense if we were originally in the antiperiodic sector then the introduc-

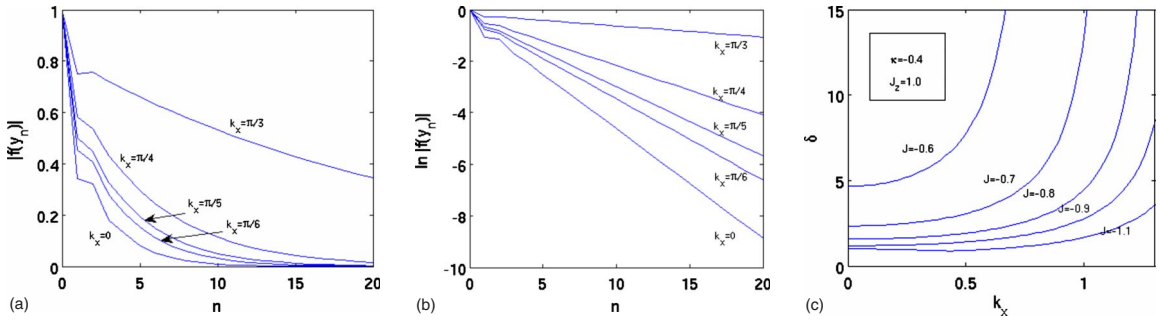

FIG. 4. (Color online) (a) The function $|f(y_n)|$ for different k_x with $J_z=1$, $J=-0.7$, and $\kappa=-0.4$. (b) A log plot of the same function $f(y_n)$ again with $J_z=1$, $J=-0.7$, and $\kappa=-0.4$. (c) The penetration depth δ as a function of k_x for different values of J and fixed J_z and κ. Penetration depth goes to infinity approximately when $|d_1+d_2|>1$.

tion of a vortex effectively restores periodicity to the dissected edge and thus allows values of $k_x=\pm 2n\pi/N_x$ to propagate along this wall.

It is worth emphasizing here that it is the number of branch cuts through a domain wall that decides if an exact zero energy mode can exist there. It is in this sense that we argue that, despite their gauge dependence, the branch cuts are more fundamental than the vortex excitations. For example, specifying that an odd number of vortices in the non-Abelian bulk only tells us that an edge mode exists on one of the boundaries but does not tell us which one. On the other hand if we specify the exact branch cut structure then we can simply infer the character of the edge modes on either domain wall.

We can extend this reasoning to deal with fully open boundaries (non-Abelian domains within Abelian domains and vice versa). However it is useful to first solve the system exactly on a hard interface $J_A=0$ where the Abelian side of the edge is the full vacuum. In this scenario numerical calculation shows that all low-energy modes satisfy $u_q=e^{i\theta}v_q$. Thus for modes along the lower edge at $y=y_0$ we have

$$a_n^\dagger=\mathcal{N}\sum_q f(y-y_0)e^{\pm ik_x x}(e^{-i\theta/2}c_q^\dagger+e^{+i\theta/2}c_q). \tag{15}$$

Note that under the conditions $k_x=0$ and $\mathrm{Im}(f)=0$ this ansatz is already a Majorana fermion. If one now substitutes this expression into Eq. (13) we observe that

$$E(J,\kappa,k_x)=\frac{8J\kappa}{\sqrt{J^2+4\kappa^2}}\sin k_x, \tag{16}$$

and that, along the bottom edge, $\theta=\tan^{-1}(2\kappa/J)$. Furthermore one sees that the function f follows from the recursive relation

$$f(y_{n+2})=\frac{1}{\sqrt{J^2+4\kappa^2}-J}[d_1 f(y_{n+1})+d_2 f(y_n)], \tag{17}$$

where

$$d_1=2J_z+2J\cos(k_x)-i2\frac{J^2-4\kappa^2}{\sqrt{J^2+4\kappa^2}}\sin(k_x),$$

$$d_2=\sqrt{J^2+4\kappa^2}+J.$$

Interestingly the structure of the mode depends on the parameter J_z but the associated energy does not. However this feature is present for the $(J_A=0)$ hard boundary condition only. Indeed numerical calculation shows that even the $\sin(k_x)$ dependence of Eq. (16) is not exact once the hard boundary condition is relaxed $(J_A,\kappa_A\neq 0)$.

The mode penetration depth can be calculated easily from the recursive relationship, Eq. (17), see, for example, Fig. 4. The most salient point is that this depth depends on k_x and therefore on E. Loosely speaking we can say that the further the energy is from $E=0$ the further it extends into the bulk. An upper limit for the momenta k_x of the edge modes can be calculated from the condition that $|d_1+d_2|<1$. Note that this condition also says that we must be inside the non-Abelian domain $|J|>|J_z|/2$ for the solution to be normalized.

V. EDGE STATES ON FULLY OPEN BOUNDARIES

If we surround a non-Abelian domain with an Abelian domain we have no zero energy states if there are no vortices inside the non-Abelian domain. If we place an odd number of vortices inside the non-Abelian domain then we do have one zero energy edge mode even though an odd number of branch cuts intersect the domain wall.

The key to understanding all this is that phases are also picked up when the wall direction is changed and that these phases all add up to π, canceling the branch cut phase. A schematic of the phases picked up for the zero mode in a rectangular shaped system is shown in Fig. 5. This picture can be arrived at by analyzing each of the edges separately and assuming the appropriate plane-wave momentum eigenstate, Eq. (15), along each edge. The trigonometric identity $\tan^{-1}a/b+\tan^{-1}b/a=\pi/2$ is the key to understanding why the total phase due to the corners is π. At this time we have been unable to fully resolve the exact behavior at the corners. However the numerically calculated example provided in Fig. 6 shows that the phase changes at a corner happen abruptly and that the momentum eigenstates structure in Eq. (15) is rapidly returned to as we move away from the corner.

The chiral (nonzero energy) edge modes are also similar to that seen on the cylinder. In these cases, as for the zero-momentum/energy modes, abrupt phase shifts are seen at the corners although in this case we cannot separate phase shifts due to momenta and those due to the corners. However it is

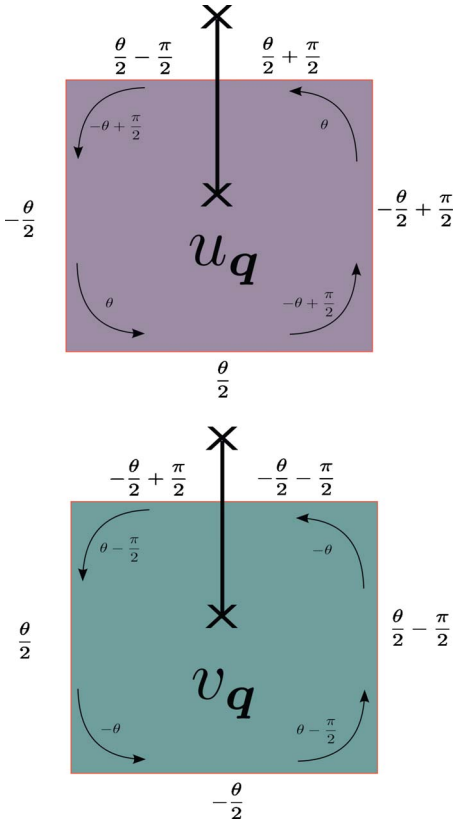

FIG. 5. (Color online) A schematic of how θ in the Majorana edge zero mode varies around an isolated domain of non-Abelian phase. In this model $\theta=\tan^{-1}(2\kappa/J)$. Inside the bulk, and at the corners, we indicate the phase that must be picked up as we move around that corner in the direction indicated by the arrows.

worthwhile to note that if we use the value of momenta measured far from the corner in expression (16) we obtain the numerically calculated energy eigenvalue for the mode exactly. This measured value of momenta is however not exactly $2\pi n/L_{Total}$ but slightly different magnitude. One could think of this as arising because the chiral mode sees a slightly different perimeter $L_{Total}-\Delta_L$ but we advise against taking this too literally.

The picture above can be immediately applied to domains of Abelian phase inside a non-Abelian one. If there is no vortex inside this Abelian domain then there is no branch cut and all modes are chiral but where the direction of the momenta for positive and negative energy modes is in the opposite sense to that on the outer edge. If an odd number of vortices exist inside the internal Abelian domain then we have an odd number of branch cuts and a zero mode can exist. As suggested by Read and Green[2] the zero mode due to a single vortex in the non-Abelian domain is special case of this scenario but where the domain edge has been reduced to a single plaquette.

For an open boundary domain, and unlike the cylindrical case mentioned above, there is now only one edge. We therefore know that it supports a zero mode if an odd number of vortices exist inside the non-Abelian bulk. As the vortex parity inside the non-Abelian domain must always equal the parity of the number of branch cuts intersecting the domain wall it would appear that there is little extra to be learned from considering the branch cuts picture in this case. However, this is only true if we insist on viewing the branch cuts as the unphysical objects whose precise form is dictated by our Jordan-Wigner string convention. If, on the other hand, we view the branch cuts as local sign changes in the coupling coefficients, then it becomes a physically measurable object, that profoundly affects the structure of the underlying fermionic system.

VI. CONCLUSION

We have analyzed edge mode structure of the Kitaev honeycomb model using a Jordan-Wigner fermionization procedure. We see that the branch cuts are naturally defined for us in both the single-particle Hamiltonian ξ and the order parameter Δ. We then extended the notion of these branch cuts to account for edge effects between Abelian and non-Abelian domains. Although our general conclusions are in agreement with other methodologies we feel there is an inherent simplicity to the above arguments that make them an important part of the overall story.

For the specific model we have chosen we have been able to derive a simple recursive relation that exactly dictates the structure on edge between a vacuum and non-Abelian domain. A number of key features are present. First the solutions are only normalized in the non-Abelian domain. Sec-

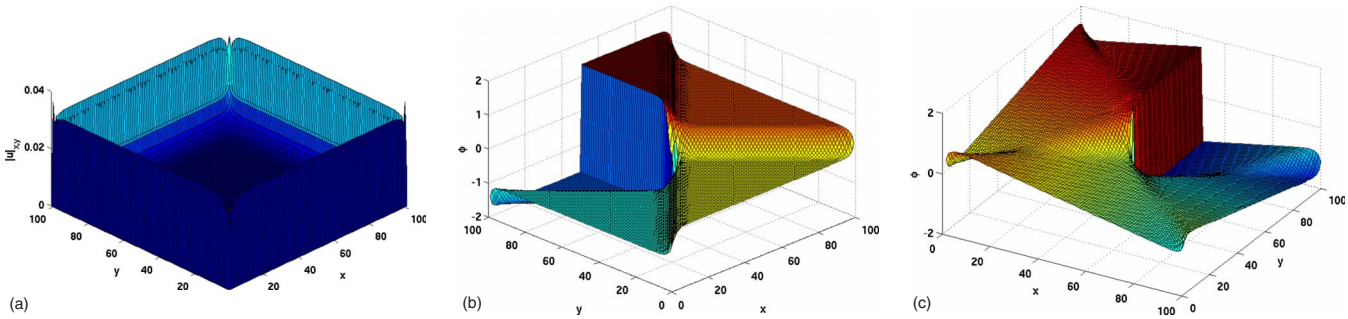

FIG. 6. (Color online) (a) The position space structure $|u_q|$ of the Majorana edge zero mode with a single vortex in the bulk. (b) The phase dependence $\phi=\theta$ for the same Majorana zero mode. (c) The phase dependence $\phi=\theta+\boldsymbol{k}\cdot\boldsymbol{q}$ for a chiral edge mode where a vortex exists in the bulk. We can see here the combined effects of the branch cut, the phase jumps at corners and the almost constant momenta $|k|\approx 2\pi/L_{Total}$. In these figures $J_x=J_y=J=-0.7$, $J_z=1$, and $\kappa=-0.4$.

ond we see a clear dependence on penetration depth on the mode momenta. We have also outlined how to apply the cylindrical solutions for the hard boundary to a fully open system.

In future work we will attempt to analyze the edge mode momentum dependency further and to extend these results to softer boundaries. We will also attempt to identify enough properties to exactly formulate the mode structure at the corners.

ACKNOWLEDGMENTS

We thank Steve Simon, Joost Slingerland, Ivan Rodriguez, and Janik Kailasvuori for interesting discussions. This work has been supported by Science Foundation Ireland through Grant No. 05/YI2/I680. J. V. acknowledges the hospitality of the Nordic Institute of Theoretical Physics (Nordita), Stockholm, Sweden.

APPENDIX

In this appendix we give a brief overview of the fermionization procedure used in Ref. 20. We begin our derivation by first noting that in Ref. 10, Hamiltonian (1) was written in terms hard-core bosons and effective spins of the z dimers using the mapping,

$$|\uparrow_{\blacksquare}\uparrow_{\square}\rangle = |\Uparrow,0\rangle, \quad |\downarrow_{\blacksquare}\downarrow_{\square}\rangle = |\Downarrow,0\rangle,$$

$$|\uparrow_{\blacksquare}\downarrow_{\square}\rangle = |\Uparrow,1\rangle, \quad |\downarrow_{\blacksquare}\uparrow_{\square}\rangle = |\Downarrow,1\rangle. \tag{A1}$$

The labels on the left-hand side indicate the spin states of the z dimer in the S_z basis. The first quantum number on the right-hand side represents the effective spin of the square lattice and the second is the hard-core bosonic occupation number. The presence of a boson indicates an antiferromagnetic configuration of the spins on a z link.

In this representation the Pauli σ operators become[10]

$$\sigma^x_{q,\blacksquare} = \tau^x_q(b^\dagger_q + b_q), \quad \sigma^x_{q,\square} = b^\dagger_q + b_q,$$

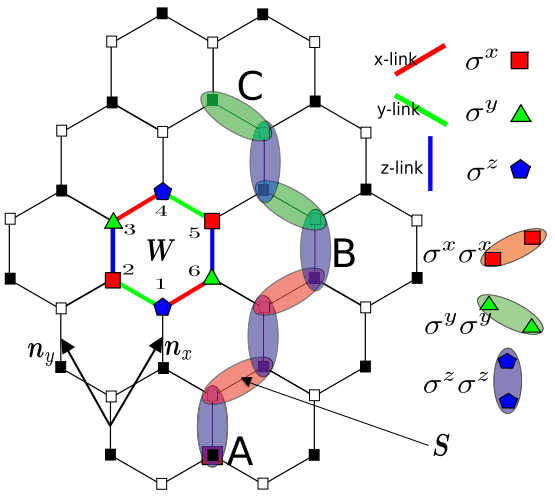

FIG. 7. (Color online) The plaquette operator W and the fermionic string S_q.

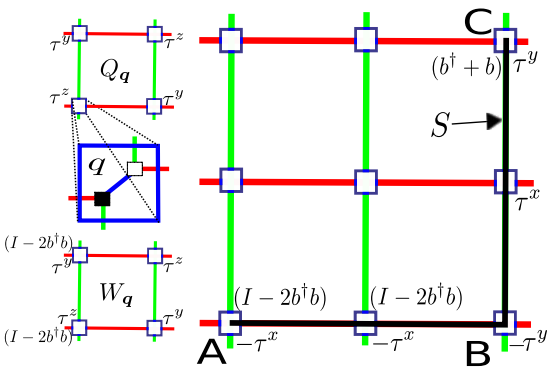

FIG. 8. (Color online) Bosonic and effective spin decomposition of the operator string S.

$$\sigma^y_{q,\blacksquare} = \tau^y_q(b^\dagger_q + b_q), \quad \sigma^y_{q,\square} = i\tau^z_q(b^\dagger_q - b_q),$$

$$\sigma^z_{q,\blacksquare} = \tau^z_q, \quad \sigma^z_{q,\square} = \tau^z_q(I - 2b^\dagger_q b_q), \tag{A2}$$

where τ^a_q is the Pauli operator acting on the effective spin at position $\boldsymbol{q}$ and $b^\dagger(b)$ are the creation (annihilation) operators for the hard-core bosons. The Hamiltonian itself becomes

$$\begin{aligned} H = &- J_x \sum_q (b^\dagger_q + b_q)\tau^x_{q\rightarrow}(b^\dagger_{q\rightarrow} + b_{q\rightarrow}) \\ &- J_y \sum_q i\tau^z_q(b^\dagger_q - b_q)\tau^y_{q\uparrow}(b^\dagger_{q\uparrow} + b_{q\uparrow}) \\ &- J_z \sum_q (I - 2b^\dagger_q b_q). \end{aligned} \tag{A3}$$

We now define a particular string operator using overlapping products of the K^α_{ij} terms of the original Hamiltonian. The primary function of the string will be to break/fix z dimers at a particular location $\boldsymbol{q}$ of the lattice, see Fig. 7. The convention is to first move along the n_x direction and then along the n_y direction until we get to the z link at $\boldsymbol{q}$. We then factor the string S_q into the effective spin and bosonic subspaces ($S = S_e \otimes S_b$) using Eq. (A2), see Fig. 8.

We identify the string S_q with the sum of fermionic creation and annihilation operators: $S_q = c^\dagger_q + c_q = (b^\dagger_q + b_q)S'_q$, where S'_q is simply the string S_q but with the bosonic dependence of the endpoint C removed, see Table I. The fermionic canonical creation and annihilation operators are $c^\dagger_q = b^\dagger_q S'_q$ and $c_q = b_q S'_q$, where the strings now enforce the intersite-fermionic anticommutator relations. Inverting these

TABLE I. The string S as four unique segments. While bosons are only created/destroyed at the endpoint C of the string, the sites in the $[A,B)$ interval also have nontrivial bosonic dependence.

	S	$S_e \otimes S_b$
$[A,B)$	$\sigma^x_{\square}\sigma^z_{\square}\sigma^z_{\blacksquare}\sigma^x_{\blacksquare}$	$-\tau^x \otimes I - 2b^\dagger b$
B	$\sigma^y_{\square}\sigma^z_{\square}\sigma^z_{\blacksquare}\sigma^x_{\blacksquare}$	$-\tau^y \otimes I$
(B,C)	$\sigma^y_{\square}\sigma^z_{\square}\sigma^z_{\blacksquare}\sigma^y_{\blacksquare}$	$\tau^x \otimes I$
C	$\sigma^y_{\blacksquare}$	$\tau^y \otimes b^\dagger + b$

expressions and substituting into Hamiltonian (A3) we get,

$$H_0 = J_x \sum_{\boldsymbol{q}} \boldsymbol{X_q}(c_{\boldsymbol{q}}^\dagger - c_{\boldsymbol{q}})(c_{\boldsymbol{q}\rightarrow}^\dagger + c_{\boldsymbol{q}\rightarrow}) + J_y \sum_{\boldsymbol{q}} \boldsymbol{Y_q}(c_{\boldsymbol{q}}^\dagger - c_{\boldsymbol{q}})(c_{\boldsymbol{q}\uparrow}^\dagger + c_{\boldsymbol{q}\uparrow}) + J_z \sum_{\boldsymbol{q}} (2c_{\boldsymbol{q}}^\dagger c_{\boldsymbol{q}} - I), \quad \text{(A4)}$$

which is the fermionic representation of the original Hamiltonian (1). The operators $\boldsymbol{X_q}$ and $\boldsymbol{Y_q}$ are related to products of loop symmetries. We restrict to particular vortex and topological sectors by replacing the operators with the eigenvalues $X_{\boldsymbol{q}} = \pm 1$ and $Y_{\boldsymbol{q}} = \pm 1$ of the sector in question.

[1] A. Yu. Kitaev, Ann. Phys. **303**, 2 (2003).
[2] N. Read and D. Green, Phys. Rev. B **61**, 10267 (2000).
[3] D. A. Ivanov, Phys. Rev. Lett. **86**, 268 (2001).
[4] A. Stern, F. von Oppen, and E. Mariani, Phys. Rev. B **70**, 205338 (2004).
[5] M. Stone and S.-B. Chung, Phys. Rev. B **73**, 014505 (2006).
[6] P. Fendley, M. P. A. Fisher, and C. Nayak, Phys. Rev. B **75**, 045317 (2007).
[7] M. Freedman, A. Kitaev, M. J. Larsen, and Z. Wang, Bull. Am. Math. Soc. **40**, 31 (2003).
[8] C. Nayak, S. H. Simon, A. Stern, M. H. Freedman, and S. Das Sarma, Rev. Mod. Phys. **80**, 1083 (2008).
[9] A. Kitaev, Ann. Phys. **321**, 2 (2006).
[10] K. P. Schmidt, S. Dusuel, and J. Vidal, Phys. Rev. Lett. **100**, 057208 (2008); S. Dusuel, K. P. Schmidt, and J. Vidal, *ibid.* **100**, 177204 (2008); J. Vidal, K. P. Schmidt, and S. Dusuel, Phys. Rev. B **78**, 245121 (2008).
[11] G. Kells, A. T. Bolukbasi, V. Lahtinen, J. K. Slingerland, J. K. Pachos, and J. Vala, Phys. Rev. Lett. **101**, 240404 (2008).
[12] J. K. Pachos, Ann. Phys. **322**, 1254 (2007).
[13] V. Lahtinen, G. Kells, A. Carollo, T. Stitt, J. Vala, and J. K. Pachos, Ann. Phys. **323**, 2286 (2008).
[14] G. Baskaran, S. Mandal, and R. Shankar, Phys. Rev. Lett. **98**, 247201 (2007).
[15] X.-Y. Feng, G.-M. Zhang, and T. Xiang, Phys. Rev. Lett. **98**, 087204 (2007).
[16] D.-H. Lee, G.-M. Zhang, and T. Xiang, Phys. Rev. Lett. **99**, 196805 (2007).
[17] H.-D. Chen and J. Hu, Phys. Rev. B **76**, 193101 (2007).
[18] H.-D. Chen and Z. Nussinov, J. Phys. A: Math. Theor. **41**, 075001 (2008).
[19] Y. Yu and Z. Wang, EPL **84**, 57002 (2008).
[20] G. Kells, J. K. Slingerland, and J. Vala, Phys. Rev. B **80**, 125415 (2009).
[21] F. A. Bais and J. K. Slingerland, Phys. Rev. B **79**, 045316 (2009).
[22] F. A. Bais, J. K. Slingerland, and S. M. Haaker, Phys. Rev. Lett. **102**, 220403 (2009).
[23] J. R. Wootton, V. Lahtinen, Z. Wang, and J. K. Pachos, Phys. Rev. B **78**, 161102(R) (2008); J. Wootton, V. Lahtinen, B. Doucot, and J. Pachos, arXiv:0908.0708 (unpublished).
[24] H. Bombin, Phys. Rev. Lett. **105**, 030403 (2010).
[25] G. Kells, D. Mehta, J. K. Slingerland, and J. Vala, Phys. Rev. B **81**, 104429 (2010).
[26] V. Lahtinen and J. Pachos, New J. Phys. **11**, 093027 (2009).
[27] G. E. Volovik, JETP Lett. **57**, 244 (1993).
[28] For classification schemes of topological insulators see, for example, Refs. 29 and 30.
[29] A. P. Schnyder, S. Ryu, A. Furusaki, and A. W. W. Ludwig, Phys. Rev. B **78**, 195125 (2008).
[30] A. Kitaev, arXiv:0901.2686, in Proceedings of the L.D. Landau Memorial Conference Advances in Theoretical Physics, Chernogolovka, Moscow region, Russia, 22–26 June, 2008 (unpublished).
[31] We will usually choose the convention that $J_z = 1$ and $J_x, J_y, \kappa \leq 0$. This convention has the advantage that our basic c fermions are associated with antiferromagnetic configurations of the z dimers and our vacua are toric code states on an effective square lattice (Ref. 20). It allows us to naturally interpret the ξ part of the BdG Hamiltonian as the single-particle equation. In momentum space we have, for example, $E_{\boldsymbol{k}} \approx c + d(k_x^2 + k_y^2)$.